FISEVIER

Contents lists available at ScienceDirect

# Science of the Total Environment

journal homepage: www.elsevier.com/locate/scitotenv



# Assessing the effects of increased impervious surface on the aquifer recharge through river flow network, case study of Jackson, Tennessee, USA



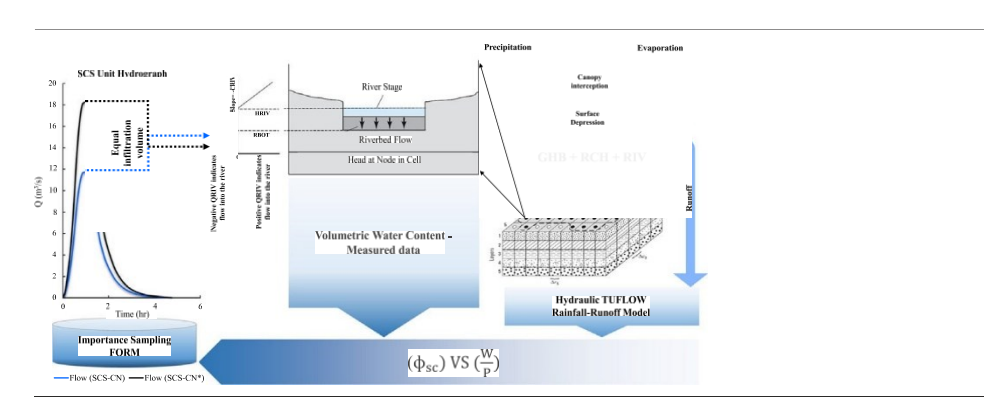
Abolfazl Nazari Giglou a,b, Rouzbeh Nazari a,b,c,\*, Farhad Jazaei d, Maryam Karimi a,b,c

- <sup>a</sup> Sustainable Smart Cities Research Center, University of Alabama at Birmingham (UAB), Birmingham, AL, USA
- b Department of Civil, Construction, and Environmental Engineering, University of Alabama at Birmingham, Birmingham, AL, USA
- <sup>c</sup> Department of Environmental Health Science, University of Alabama at Birmingham, Birmingham, AL, USA
- d Department of Civil Engineering, the University of Memphis, Memphis, TN, USA

#### HIGHLIGHTS

- Water permeability and depth simulated with and without the probability distribution function.
- The modified SCS-CN approach improved the results through the basin FORM factor.
- Construction design using the modified SCS-CN method provides more safety.
- Quantification of hydrologic responses due to urbanization using TUFLOW.

#### GRAPHICAL ABSTRACT



## ARTICLE INFO

Editor: Jurgen Mahlknecht

Keywords: Urbanization Soil wetting ratio Soil water storage index TUFLOW SCS-CN Aquifer recharge Flood management

## ABSTRACT

Understanding pathways connecting urbanization to the recharge process across the land surface and river environment is of great significance in achieving low-impact development. Accordingly, the contribution of an urbanized region with a low and high development rate, along with the expected overflow into the river netresulting from increased impervious surfaces, was assessed in the recharge rate at Jackson, Tennessee. To this end, first, the losses were calculated using the standard and modified SCS-CN methods for the maximum probable flood condition. Then, TUFLOW was applied to simulate the two-dimensional flood for a historic 24-h probable maximum precipitation event with a 100-year return period. The results of TUFLOW were later calibrated using the results of standard and modified SCS-CN methods. A calibrated MODFLOW was employed to assess the effects of urbanization and, consequently, the plausible extended river network on the recharge rate. Results revealed that the West Wood contribution in groundwater recharge was 19 % less than the Musa Street, while it supplies approximately 2.7 % more flow than Musa Street. The performance evaluation results of TUFLOW showed 0.4916 and 0.689 as Nash-Sutcliffe, respectively, for the standard and modified SCS-CN methods. Although the flow velocity and depth were respectively increased by 3.3 % and 8.3 % under modified SCS-CN compared to the standard one, the soil water storage capacity remained constant at equal to 0.16 mm. Results revealed that the maximum soil water storage capacity was fulfilled soon through the modified SCS-CN than the standard method leading to higher flood volume and discharge. To this end, the discharge resulting from modified SCS-CN was approximately 1.5 times higher than that in the standard method under the same precipitation condition. Our findings suggest that designing any construction, mainly dams downstream, based on the modified SCS-CN estimations will provide more safety, particularly in crowded regions. Also, overflowing the excess surface runoff into the river network resulted from the increased

<sup>\*</sup> Corresponding author at: Sustainable Smart Cities Research Center, University of Alabama at Birmingham (UAB), Birmingham, AL, USA. E-mail address: rnazari@uab.edu (R. Nazari).

impervious surface amplifying the flow volume, depth, and velocity across the river networks, finally leaving the area without increasing the aquifer's recharge rate. The results provide insights into possible sustainable development options and flood management in the built-up area.

#### 1. Introduction

There is no doubt that groundwater is one of the most important resources in terms of the supply of fresh water for socio-economic development around the world. Unsustainable socioeconomic development, land and climate changes and prolonged droughts are among the factors affecting groundwater resources' quantity and quality. Another stimulus is urbanization, which has increased pressure on groundwater resources from several perspectives (Nazari et al., 2013; Feng et al., 2021; Pasquier et al., 2022). On the one hand, urbanization, and subsequent wellfield developments have significantly increased groundwater withdrawal (Jazaei et al., 2019; Ayalew Yifru et al., 2022). On the other hand, urbanization increased impervious surfaces and, thus, changed the surface flow regimes and aquifer recharge mechanisms (McGrane, 2016; Feng et al., 2021; Pasquier et al., 2022). The increased impervious surfaces have challenged the aquifer recharge rate in the built-up region leading to increasing catastrophic hazards such as flash floods and degradation of water qualities (Guan et al., 2016; Rosburg et al., 2017; Fahad et al., 2020; Lü et al., 2022; Ayalew Yifru et al., 2022; Kumar et al., 2022; Talebmorad and Ostad-Ali-Askari, 2022).

Water infiltration and groundwater recharge can occur through saturated beds of surface water bodies (e.g., lakes, streams, and creeks) and through unsaturated vadose zones (Lerner et al., 1990; Healy and Cook, 2002; Scanlon et al., 2002). The infiltration process is strictly affected by topographic conditions and biophysical features, mainly land use at the basin (Bartlett et al., 2016; Karimi et al., 2017; Ostad-Ali-Askar, 2022; Fathi Nafchi et al., 2021; Shirmohammadi et al., 2020). Impermeable surfaces in urban areas drive excess overland flow into the hydrographic network, causing runoff of greater intensity and extent. Thus, urbanization can intensify the river network and change the runoff properties (shape and volume) downstream urban areas. Several methods have been developed by various research groups to estimate surface runoff. However, accurate estimation of runoff losses remains one of the main sources of uncertainty. By simplifying assumptions, such as considering the same soil wetting conditions throughout the entire basin, runoff losses are often misestimated (Wang, 2018). Accurate estimation of the soil wetting extent during rainfall events is critical to determining the overland flow network extent and magnitude, leading to accurate urbanization impact assessment.

The Conservation Service Curve Number (SCS-CN) is the widespread approach to estimating surface runoff (Mockus, 1972; Shi and Wang, 2020; Schoener and Stoneb, 2019; Lian et al., 2020). In this approach, soil-wetting conditions only include fixed and limited amounts of runoff under wet, dry, and medium conditions. The initial soil water storage was considered 20 % of the basin's total storage capacity (HEC, 2020). Even though recently developed models can assess soil moisture ratios, the uncertainty imposed by effective precipitation estimation on hydrograph components led to the localization of the SCS-CN method (Schoener and Stoneb, 2019; Lian et al., 2020). Most errors in the estimation of the maximum discharge across large catchments are referred to computing water percolation into the soil during historic flood conditions (Wang, 2018). Thus, SCS-CN usually overestimates maximum discharges by using simplistic assumptions in estimating the soil moisture compared to in-situ data, specifically in large catchments (Wang, 2018).

The most comprehensive study addressing the SCS-CN estimation challenges was conducted by Wang (2018), which resulted in a new SCS-CN equation. According to Wang's (2018) equation, a probabilistic distribution is necessary to calculate the overland flow under boundary conditions (i.e., upper and lower bounds of soil storage index). In this Equation, runoff is estimated only for the affected basins, and the results are modified according to the topographic conditions of the catchments.

Several models have been developed to assess the effects of impervious surfaces on groundwater recharge rate in urban areas, such as GSFLOW, ParFLOW, HydroGeoSphere, MIKE SHE, MODHMS, and SWATMOD. These models have been widely used to address several water resources challenges, including surface-groundwater interactions (Huntington and Niswonger, 2012), irrigation management (Perez et al., 2011), water quality, land use, and climate change impacts on water resources (Markstrom et al., 2008; Tian et al., 2015). Most of them use MODFLOW code to model subsurface water systems due to their high performance in capturing groundwater system properties accurately. However, one of the efficiently accurate runoff simulations can be fulfilled by coupling the SCS-CN method with a runoff simulation model such as TUFLOW, which would be considered as this novelty.

This study aimed to assess the effects of increased impervious surfaces on the recharge rate in the built-up area using a coupled SCS-CN-TUFLOW approach. This approach established an accurate relationship between soil wetting conditions and soil storage index in order to reduce the uncertainty in the estimation of runoff volume and recharge rate. Finally, the effects of increased impervious surfaces and, consequently, the expected excess overland flow on groundwater recharge were assessed using MODFLOW.

#### 2. Materials and methods

#### 2.1. Study area

The study area is located in Jackson, Tennessee, and extends between 88° 47′ 30″ to 88° 50′ 00″ W longitude and 35° 38′ 00″ to 35° 39′ 30″ N latitude. It is part of the Memphis Aquifer recharge area belt that supplies fresh water for municipal and industrial usage (Fig. 1). Fig. 1 shows two distinct areas, Sandy Creek West Wood and Sandy Creek Muse Street, which indicate high and low urban development, respectively. These areas resemble biophysical characteristics but differ in urban development, making it ideal for studying how urbanization would recharge.

The slopes in both areas are very low, and surface flow occurs temporarily following rainfall events. In this area, the rainfall is highest during February–March and lowest during September–October, respectively. Relatively low slopes, along with effective urban uses with scattered streams, allow for studying the effects of urbanization and therefore increased impervious surfaces on the hydrological process and flow network.

#### 2.2. The groundwater and surface water model development

The TUFLOW, grid-based 2D hydrodynamic model for free-surface flow, was applied to estimate the accurate amount of overland flow using the standard and modified SCS-CN methods, which was of utmost importance in this research. As an urban hydraulic runoff model, TUFLOW can capture complex two-dimensional flow components individually (WBM, 2016; Fahad et al., 2020). TUFLOW is a distributed hydrological model used to analyze runoff risk management which is differentiated from the other 2D flood models through the inclusion of the viscosity or sub-gridscale turbulence (WBM, 2008, 2016). It is mainly used to simulate freesurface flows and inundation patterns in floodplains, coastal areas, estuaries, rivers, and urban areas (WBM, 2016). SCS-CN and its newly modified version by Wang (2018) were employed to capture the relationship between soil moisture ratio and soil storage index. In the modified SCS-CN, a new distribution function is proposed as a substitute for the upper bound of soil water storage conditions to better capture the spatial distribution of soil water storage capacity (Wang, 2018). Thus, it is necessary to

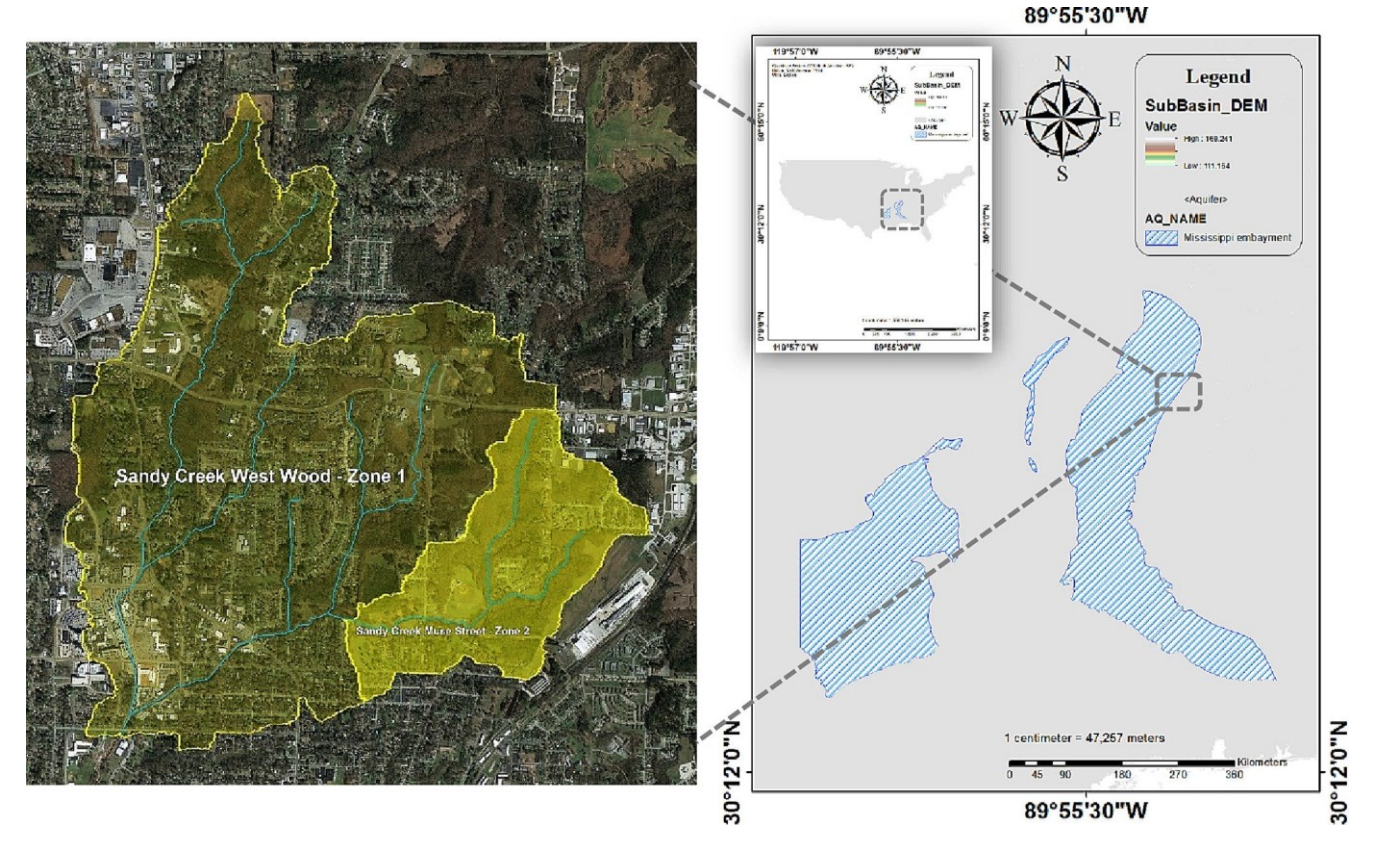


Fig. 1. The study area location (source: Environmental Systems Research Institute (ESRI)).

simulate surface runoff twice under two different soil wetting conditions (i.e., standard and modified SCS-CNs). This allows for determining how the basin First Order Reliability Method (FORM) factor, along with the probability distribution function, affects the hydrological response throughout the basin. The modified SCS-CN method can precisely address the challenges that arise from the simplification assumption. The modified SCS-CN approach can minimize the unintended effects of simplifying assumptions (i.e., soil wetting condition and Basin's soil water storage

capacity) on misestimating soil wetting conditions. Thus, using the modified SCS-CN would improve the results of TUFLOW and lead to a more accurate runoff projection (see detailed model explanation in Wang, 2018) The overland flow volume and its distribution for the historic Probability Maximum Precipitation (PMP) event were performed under the two soil wetting conditions using the standard and modified SCS-CN method. First, the probable maximum precipitation with a 100-year return period was estimated using the Bell equation (Eq. (1)). Then, the precipitation

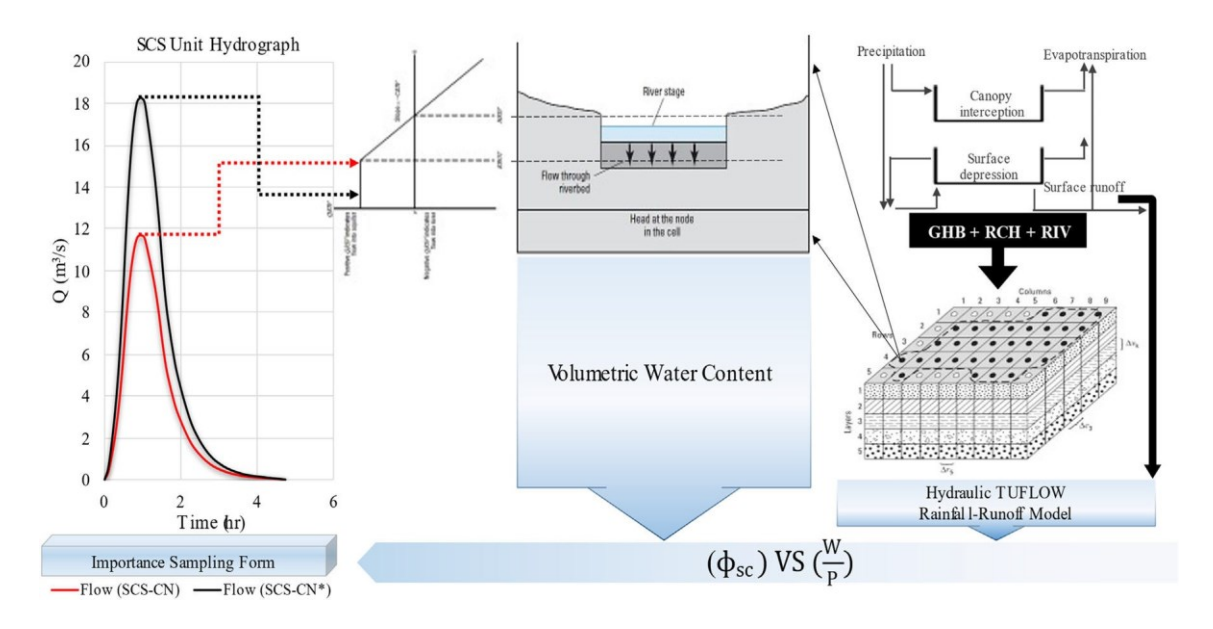


Fig. 2. The conceptual model of aquifer recharge fluctuations from the river network as a result of increasing impermeable surfaces for the two standards and modified SCS-CN methods (SCS-CN\*: modified, Wang, 2018).

distribution pattern was developed based on the SCS Type III. The standard and modified SCS-CN methods were used to analyze the sensitivity of maximum flow volume to variation in FORM factor and soil wetting conditions (Wang, 2018).

$$P_T \frac{1}{4} \delta 0:21 \ln T \circ 0:52 \circ 0:54 \ell^{0:25} - 0:5 P_{\phi}$$
 (1)

where t is the rainfall duration (min), T is the return period (year),  $P_0^{\rm r}$  is the precipitation amount received in an hour with a 10-year return period (min) and  $P_T$  is the precipitation amount received in t minutes with a T-year return period.

Fig. 2 depicts the developed conceptual model to simulate the flow-forming process and dynamics across the basin and river network environment using the two standards and modified SCS-CN methods. The figure illustrates how the accurate estimation of losses during rainfall events can affect the results, mainly runoff peak.

A TUFLOW model was developed to simulate flood conditions under a historic rainfall event with a 100-year return period, which was developed through SCS artificial hyetograph. The model was calibrated using the verified flood volume derived from the SCS-CN modified equations (Wang, 2018). Then, the flow component, the runoff depth distribution, was used to estimate the spatially distributed soil water capacity within the basins. A performance function was defined based on the first-order reliability method (FORM) to employ the sensitivity analysis. This was performed by defining a performance function in the probability distribution domain and calculating the failure threshold using the soil moisture ratio and soil storage index derived from TUFLOW and SWC (Soil Water Content) sensors data. Fig. 3 provides an overview of the key stages of the methodology. Using the SCS-CN method, the shape of the flow network was explored using the probabilistic distribution of losses in the runoff volume hydrograph.

A calibrated modeling approach was used to quantify the effects of impervious surfaces on recharge rate. The 3D groundwater flow model in

20 vertical layers with a cell size of 10\*10 m was developed using the MODFLOW code. The artificial neural network of LSTM was employed to predict precipitation from September 2017 to December 2023 as a recharge source for the last 36 months of the modeling period. This timeframe was considered due to the availability of reliable water level data. In addition

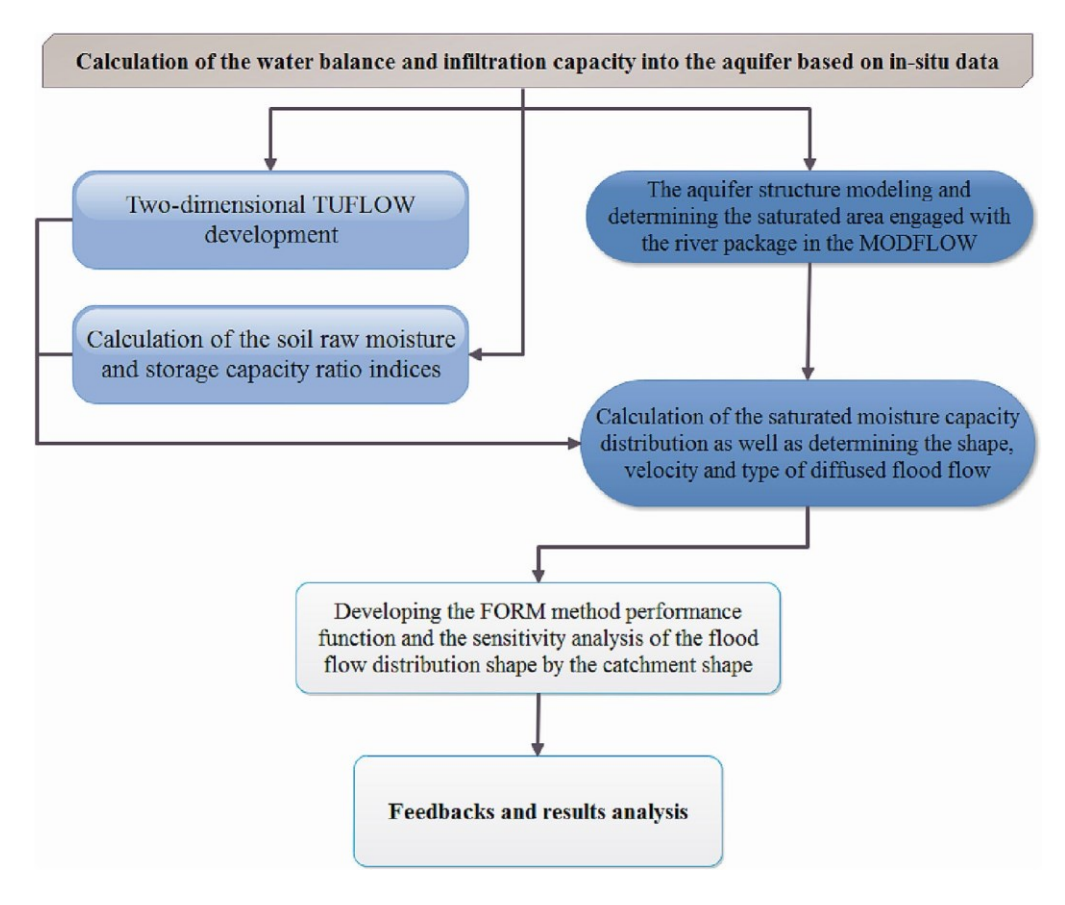
to four exploitation wells, the area involves permeable boundaries in the north and south parts of the aquifer. The recharge variations were calcu-

lated using monthly observed precipitation, evaporation, and outflow datasets measured across the region. The monthly average values were applied to the conceptual model based on land use types and impermeable surfaces percentage. The RIV package of MODFLOW was implemented with and without recharge components to separate the total recharge from the leakage from the riverbed. This way, the recharge volume from river networks is specified by the actual ratio of the observed storage, indicating the contribution of river networks to the region's total recharge.

Also, the two-dimensional flood hydraulic depth and the impermeability percentage of different land use types were used to calculate the soil wetting ratio and soil storage index. These indices were then applied to develop the study area's soil water storage capacity distribution. The saturated moisture capacity captures the amplitude changes of the flow network and, consequently, the aquifer recharge status in response to the changes in flood flows. The basin soil water storage capacity was determined more accurately due to the extensive network of finite difference approaches in TUFLOW. Therefore, the difference in soil water storage capacity during the two model runs implied how flood variations can affect the recharge process into the aquifer.

#### 2.3. Soil water storage capacity

The average flow depth was determined using TUFLOW for a historical event (100-years return period simulated within a 10\*10 m cell size) from its initiates to reach the peak at the outlet, total in 13 steps (6 min). The overland flow volume was estimated using modified SCS-CN (Wang,



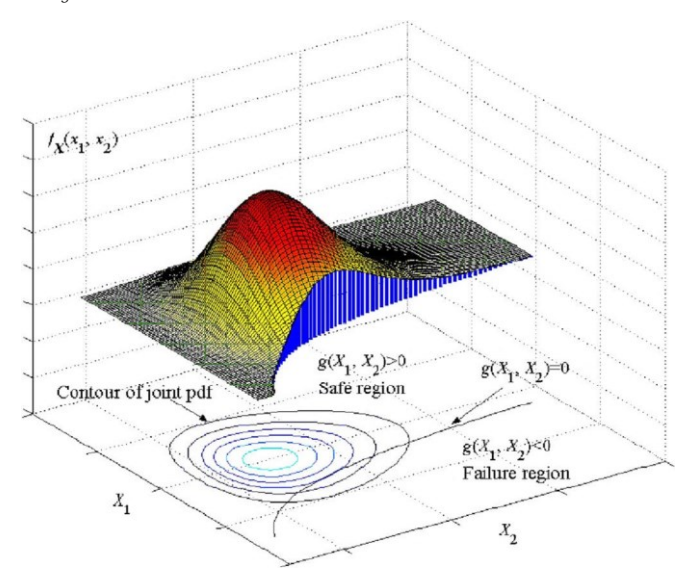
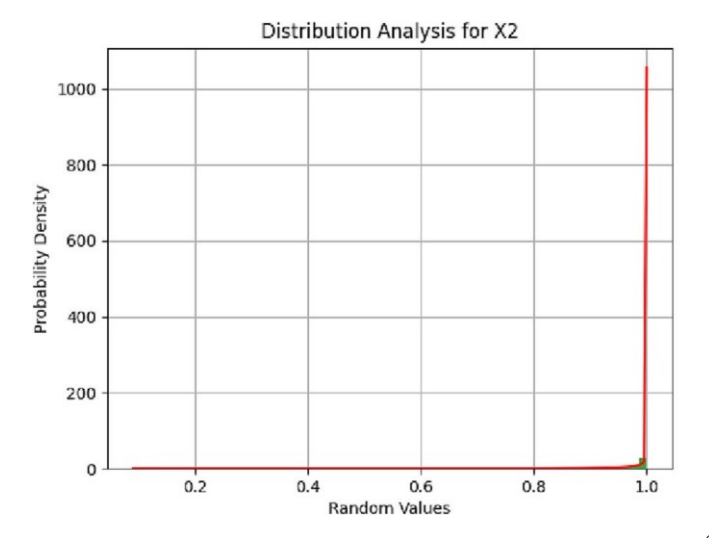


Fig. 4. Probabilistic integral of two random variables in three-dimensional space (Faber, 2009).

2018) across the region, leading to the new peak flow. The modified SCS-CN determines the distribution of the soil water storage based on a probability function distribution. Therefore, Wang's (2018) equation estimates the overland flow closer to reality and greater than the standard SCS-CN equations concerning historical flood events. The magnitude of the computational value with a reasonable threshold can face the soil water storage capacity of the basin with challenges through reprocessing the standardized layers, including the standardized flood flow depth, impermeability, and soil retention capacity distribution coefficient. Therefore, once a probabilistic value for the form factor (a) was achieved through the Wang (2018) equation, the moisture ratio as a representative of the soil water storage was estimated in two ways: 1- based on the modified SCS-CN approach results which work based on the point probability distribution function at the basin scale, and 2- based on the standard SCS-CN approach results. Eq. (1) was employed to calculate the basin form factor of the modified SCS-CN method (Wang, 2018).

$$\frac{W}{P} \frac{\Phi_{sc \, \delta SSWP} - \frac{P_{\uparrow}^{2}}{P}}{1 \, p \, \Phi_{sc \, \delta SSWP} - 2 \frac{W_{i}}{P}}$$
 51b



where the soil storage index ( $\Phi_{sc}$  (SSW)) was calculated based on VWC observed data using Eq. (2). According to Eq. (2),  $\Phi_{sc}$  (SSW) was calculated close to reality using  $\Psi$  index (Wang, 2018).

$${}^{\underline{\Phi}_{\text{sc}}} {}^{\underline{S_b}} {}^{\underline{N}} {}^{\underline{N}} {}^{\underline{D}} = \Psi^{\underline{b}}$$

where, S<sub>b</sub> is the region's maximum average soil water storage capacity. According to the basic assumption of the SCS-CN method, the antecedent moisture (w<sub>i</sub>) was considered equal to 20 % (Ponce, 1996) of the total average storage capacity of the basin (Eq. (3)) (Wang, 2018).

$$w_i \frac{1}{4} 0:2 \times \psi_{\delta SCS - CNP}$$
 (3)

According to Eq. (4), the modified SCS-CN was applied to extract the observed values from the moisture ratio, which accurately estimates under historical flood conditions (Wang, 2018).

$$\frac{W}{p^{\frac{1}{2}}} = \frac{1}{1} \frac{\frac{1}{p} \frac{\frac{1}{p} - 2am}{\frac{1}{p} - 2am}}{1 - \psi} = \frac{1}{1} \frac{\frac{m}{p} \frac{1}{1}}{\frac{1}{p} - \frac{1}{q}} = \frac{2a}{1 - \psi} \frac{\frac{2}{p} \frac{2m}{m} \frac{2$$

where, m is calculated based on two variables a, and  $\psi$  which is varied between 0 and 2 (Wang, 2018). This parameter (m), which has considered as  $\beta$  by Wood et al. (1992), was estimated between 0.01 and 5 in this study, indicating the convexity and concavity of the soil storage capacity distribution curve. Determining the graphic sensitivity value between the soil storage index and soil moisture ratio can lead to the improvement of the accuracy of basin form factor (a) in the modified SCS-CN equation (Eq. (5)) (Wang, 2018).

According to Eq. (5), the surface runoff is a function of precipitation (P), the maximum value of average soil water storage capacity over the basin (S<sub>b</sub>), the shape parameter of the storage capacity distribution (a), storage capacity distribution (m) and initial soil moisture ( $\psi$ ) (Wang, 2018). In this Equation, estimating the shape parameter of the storage capacity distri-

bution (a) is similar to the Cp parameter in the Schneider hydrograph, which was calculated using trial and error by the observed data (Eq. (6)). Its initial approximation in this study was calculated through the

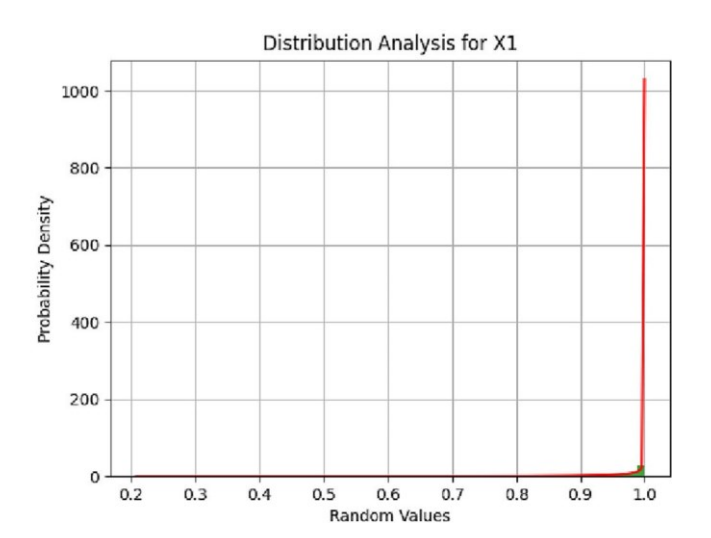


Fig. 5. Beta distribution based on statistical characteristics of the soil water storage index and soil moisture ratio.

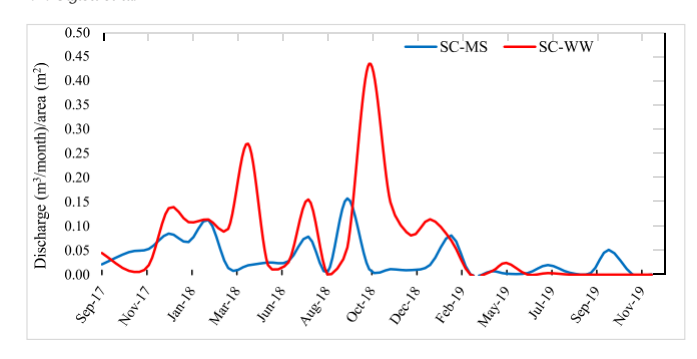


Fig. 6. The monthly temporal discharge distribution per unit of area across the studied watersheds.

equivalence assumption between the discharge obtained by the standard and modified SCS-CN methods (Eq. (7)) (Wang, 2018).

$$\begin{array}{c}
m \frac{1}{4} \underline{\psi \delta 2} - \underline{a}\underline{\psi}\underline{b} \\
2\delta 1 - \underline{\psi}\underline{b}
\end{array}$$
(6)

$$\Phi_{\text{sc }\delta\text{Model}} 
\begin{array}{c}
\sqrt{2b - S_0} \sqrt{2b} \\
P
\end{array}$$
(7)

where So is the initial soil water storage at the begging of the rainfall event. The  $\Phi_{sc\ (Model)}$  was calculated using the TUFLOW results as presented in Eq. (7).

## 2.4. First-order analysis of the basin shape reliability

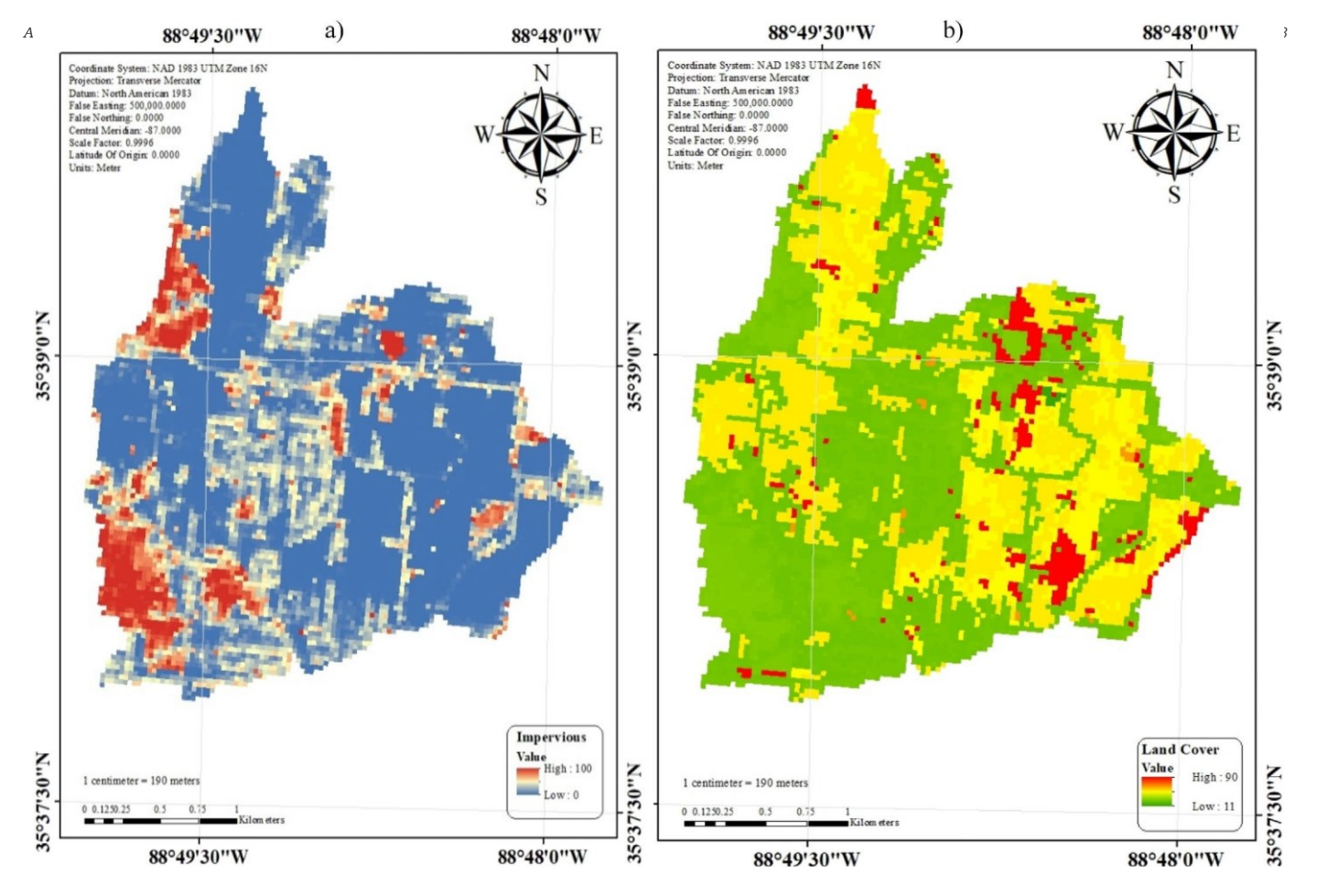
Determining the reliability threshold in a performance function of an event magnitude was accomplished to specify the threshold of reliability of the basin form factor (a) in the estimation of surface runoff in the unit hydrograph of the modified SCS-CN equations. The reliability is defined as the positivity of the significant function of g (X), when  $P \{g(X) > 0\}$ . In other words, reliability is the probability that the random variable of X = (X1, X2..., Xn) is in the safe region of g (X) > 0 (Fig. 4).

Therefore, the failure probability is defined as g (X) <0. Considering the probability density function of the variable X as  $f_x(X)$ , the probability of failure is evaluated by Eq. (8) (Faber, 2009).

Ζ

The first-order reliability or FORM (First Order Reliability Method) analysis is originally derived from the significant function of g(X), which is linearly approximated by the Taylor expansion (Melchers, 1999). The probabilistic integral Eq. (8) is visualized in two dimensions. Integral simplification is performed by transferring or converting a dependent random variable space into a standard space as an independent random variable

space (Melchers, 1999). This space contains the main variable of X = (X1, X2..., Xn), called X space. All random variables of X = (X1, X2, Xn) are converted from X space into standard space to convert the integral contours of the f(X) in an organized and symmetrical manner. While the standard variables of U = (U1, U2..., Un) have a certain distribution. In



 $Fig.\ 7.\ a)\ Impermeability\ surfaces\ map\ across\ the\ study\ area,\ b)\ Land\ cover\ variety\ map\ across\ the\ study\ area.$ 

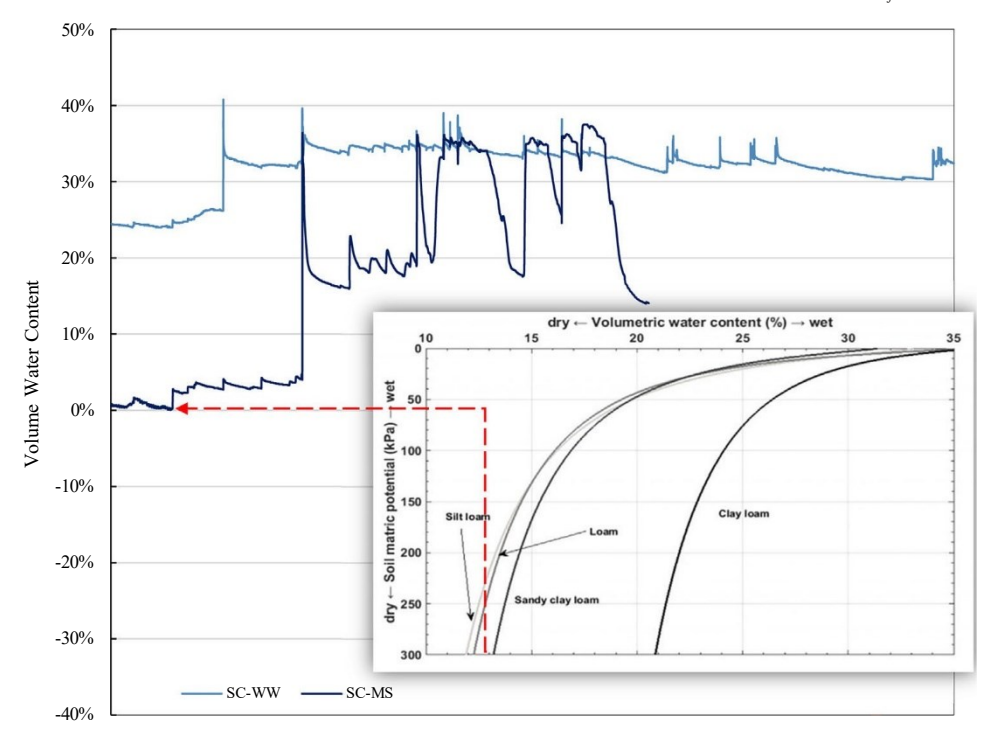
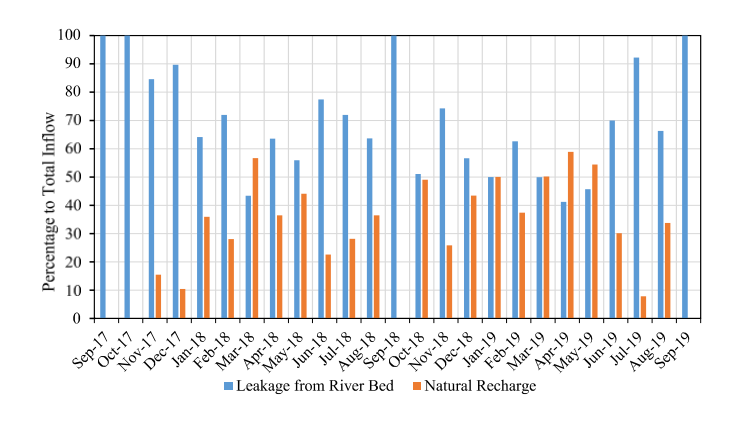


Fig. 8. The basic distribution pattern of soil saturation percentage and the observed VWC values at WW and MS.

this case, the converted space is called U space. Eventually, the probabilistic integral will be equal to Eq. (9) (Faber, 2009).

Fig. 5 illustrates the Beta statistical distribution for X1 and X2 parameters obtained by the established distributions in the performance function of the reliability analysis. (16) The statistical distribution (Fig. 5) for all states of form factor (a) showed that the closest fit occurs with the probabilistic beta distribution. The Beta continuous distribution includes two free parameters on the interval [1 and 0],  $\alpha$  and  $\beta$ . The closest fit to the data was fulfilled around  $\beta$  = 1 and  $\alpha$  = 5. The probability density function of this distribution was presented in Eq. (10).

$$x^{\alpha-1}$$
ð 1 þ  $x^{-\alpha-\beta}$  föxþ 1/4  $\frac{b}{B\eth\alpha_{\beta}b}$   $\eth$  10þ



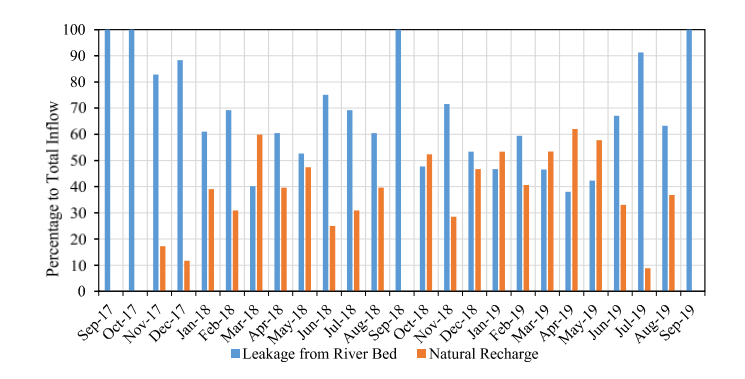


Fig. 10. Contribution of the recharge components into the aquifer at Westwood watershed zone.

The shape of the sub-integral function was simplified to development of

further probabilistic integrals for evaluation leading to the approximation of the boundary integral of g(U)=0. In this section, the FORM method uses a linear approximation called the first-order Taylor expansion analysis, as presented in Eq. (11).

gðUÞ 
$$\approx$$
 LðUÞ ¼ gðu Þ þ  $\nabla$  gðu ÞðU $-$ u Þ $^{\mathrm{T}}$  ð11Þ

where L(U) is the linearized significance function,  $u^* = (u^*_1, u^*_2, ..., u^*_n)$  is the design point, T is the conversion base and  $\nabla g$  ( $u^*$ ) is the slope of the g (U) function at the  $u^*$ . The expansion of the significant function was considered at the point with the greatest amount of the sub-integral function, which is known as the maximum probability density. The point with

Table 1 Comparison of leakage percentage from the riverbed and natural recharge.

Watershed	Leakage from Riverbed to Total	Natural Recharge to Total
Zone	Inflow (%)	inflow (%)

A.N. Giglou et al. Fig. 9. Contribution of the recharge components into the aquifer at Muse Street watershed zone.

Muse Street Zone Westwood Zone 70

67

Science of the Total Environment 872 (2023) 162203

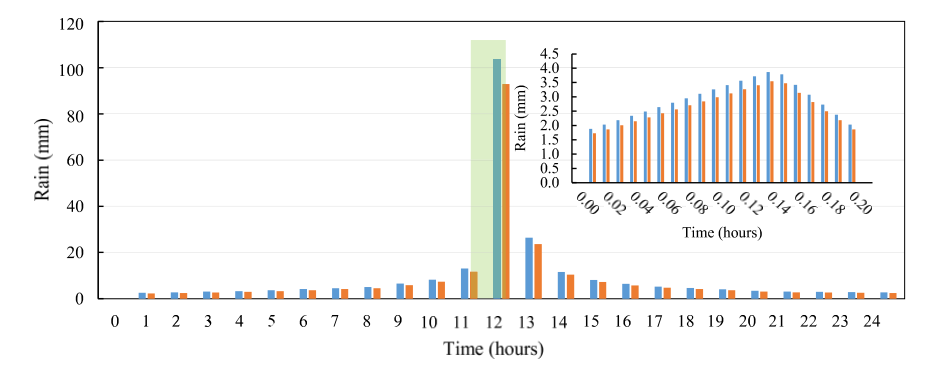


Fig. 11. The SCS Type III Hyetograph along with the specified value at the proposed SCS-CN dimensionless hydrograph.

the highest probability density at the significant function of g(U) = 0 is the Most Probable Point (MMP). Eq. (12) was applied to capture this coordinate.

The processes to calculate the FORM factor can be summarized in 3 steps (Faber, 2009): 1- converting the main random variable from X space to U space using the Rosenblatt transform; 2- searching the MPP in U space and calculating the  $\beta$  reliability index; and 3- calculation of reliability  $R = \phi (\beta)$ .

The Importance Sampling method was employed to capture the uncertainty threshold of the shape parameter (a) dynamics using the mean values and standard deviation specified for the two variables of X1 and X2. This way, the probabilistic assessment of calculated discharge was possible using the standard SCS-CN distribution method based on an evaluation performance function.

Uncertainty resulting from incomplete information usually arises during practical computational molding, affecting results and leading to uncertain performance (Wang et al., 2013: Wang, 2018). Due to the dense form of the distributed data across the random values, a sampling method was applied to estimate results more accurately. In statistics, Importance Sampling (IS) is a general technique for estimating the properties of a particular

distribution, while only the samples that differ from the basic distribution are produced. This method was first presented by Kloek and Dijk (1987) and applied to reduce the number of simulations and the coefficient of variation. Importance Sampling (IS) is one of the widespread methods where its characteristics regarding failure level were added using Eq. (13).

where  $h_x$  (X) is the probability density function of the Importance Sampling (Faber, 2009), selecting the  $h_x$  (X) is the key factor in this method, where the samples are mainly obtained from the failure domain. To this end, a FORM analysis is often performed to find a previous breakpoint (Baker, 2010) which was defined as X2-X1 in this study. The processes for the FORM reliability calculations were accomplished using the Importance Sampling in Python 3.8.

#### 3. Results and discussion

#### 3.1. Ground and surface water models

Results showed that the contribution of West Wood contributes in the recharge process was 19 % less than Muse Street. While the water supply through river networks in the West Wood, approximately 2.749 %, was higher than that in Muse Street drainage system. Fig. 6 illustrates the response of the studied watershed ((m³/month)/m²) regarding the received precipitation over the study period. According to this figure, the SC-WW watershed significantly contributed to the surface runoff

 $\begin{tabular}{ll} Table 2 \\ The Initial Losses and Continues Losses corresponds to the different land cover types with different percentage of impervious surfaces. \\ \end{tabular}$ 

Land Cover type	IS	TUFLOW Run-1			TUFLOW Run-2		
		IL (mm)	CL in Base time	CL (mm/h)	IL (mm)	CL in Base time	CL (mm/h)
Open Water	0.000 %	0.76	34.19	180.40	15.46	30.76	162.33
Developed, Open Space	8.405 %	0.70	31.32	165.24	14.16	28.18	148.68
Developed, Low Intensity	33.199 %	0.51	22.84	120.51	10.33	20.55	108.44
Developed, Medium Intensity	61.290 %	0.29	13.23	69.83	5.98	11.91	62.84
Developed, High Intensity	86.235 %	0.10	4.71	24.83	2.13	4.23	22.34
Barren Land (Rock/Sand/Clay)	0.000 %	0.76	34.19	180.40	15.46	30.76	162.33
Deciduous Forest	0.000 %	0.76	34.19	180.40	15.46	30.76	162.33
Evergreen Forest	0.000 %	0.76	34.19	180.40	15.46	30.76	162.33
Mixed Forest	0.000 %	0.76	34.19	180.40	15.46	30.76	162.33
Shrub/Scrub	0.000 %	0.76	34.19	180.40	15.46	30.76	162.33
Grassland/Herbaceous	0.000 %	0.76	34.19	180.40	15.46	30.76	162.33
Pasture/Hay	0.000 %	0.76	34.19	180.40	15.46	30.76	162.33
Cultivated Crops	0.000 %	0.76	34.19	180.40	15.46	30.76	162.33

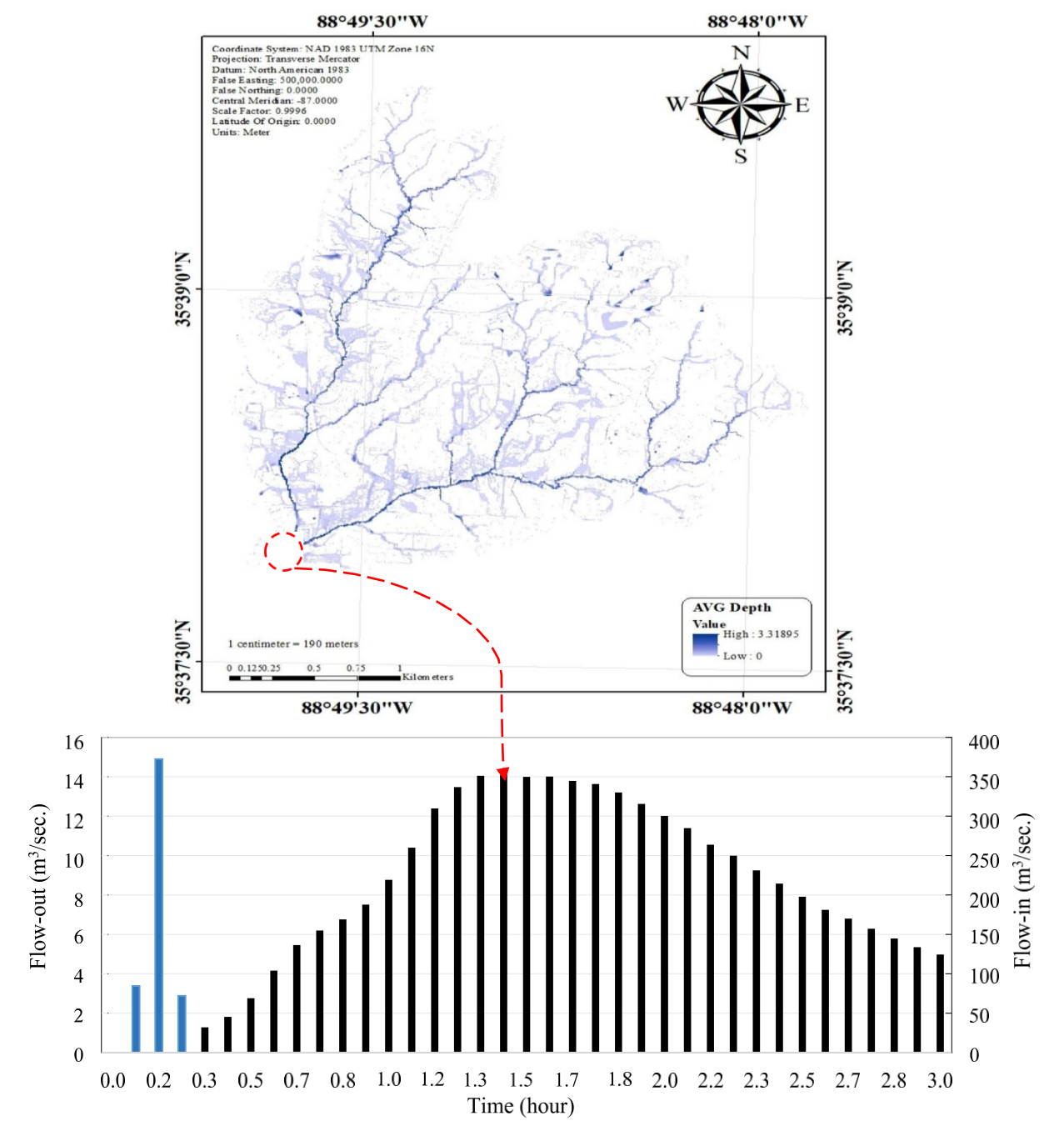


Fig. 12. Temporal flood distribution and hydrograph in the hydraulic model initial implementation at WW.

generation than the SC-MS while receiving approximately the same precipitation. This figure carries an important message regarding gener- ated surface water per unit of area, which is an important topic in urban hydrology, mainly flood control.

The results suggest that the peak flow in SC-WW was higher than the SC-MS where its reach at own maximum (approximately  $0.43~(m^3/month)/m^2$ )) in October 2018. Fig. 7a and b show the spatial impermeability coefficient and land cover variability across the study area. This information was collected from USGS datasets which were later updated for the study area using GIS. The impermeability factor was classified between 0 and 100 %, where the red color indicates the most impermeable areas across the study area (Fig. 7a). The land cover variability map, which mostly carries the land surface roughness and, therefore, Manning's roughness coefficient (Ryan et al., 2022), was applied to

simulate flow through TUFLOW (Fig. 7b). According to these figures, the distinct parts of the West Wood zone upstream and outside the do-main of the Muse Street zone have not practically contributed to the aquifer recharge during the flood event.

Basin water storage capacity, the amount of water stored in the soil, depending on the soil type and texture, generally follows the distribution pattern presented in Fig. 8. This figure depicts the basin soil storage capacity dynamics recorded at 15-min intervals using SWC sensors embedded in boreholes. The maximum amount of 40 % was shown as the basin storage capacity in the proximity of the SWC sensor, located at the downstream part of the West Wood zone. Since this region benefits the areas within by near-zero permeability, based on Fig. 7, which illustrates 13 % as the minimum soil water storage capacity, 1 % was considered for the standardization of layers.

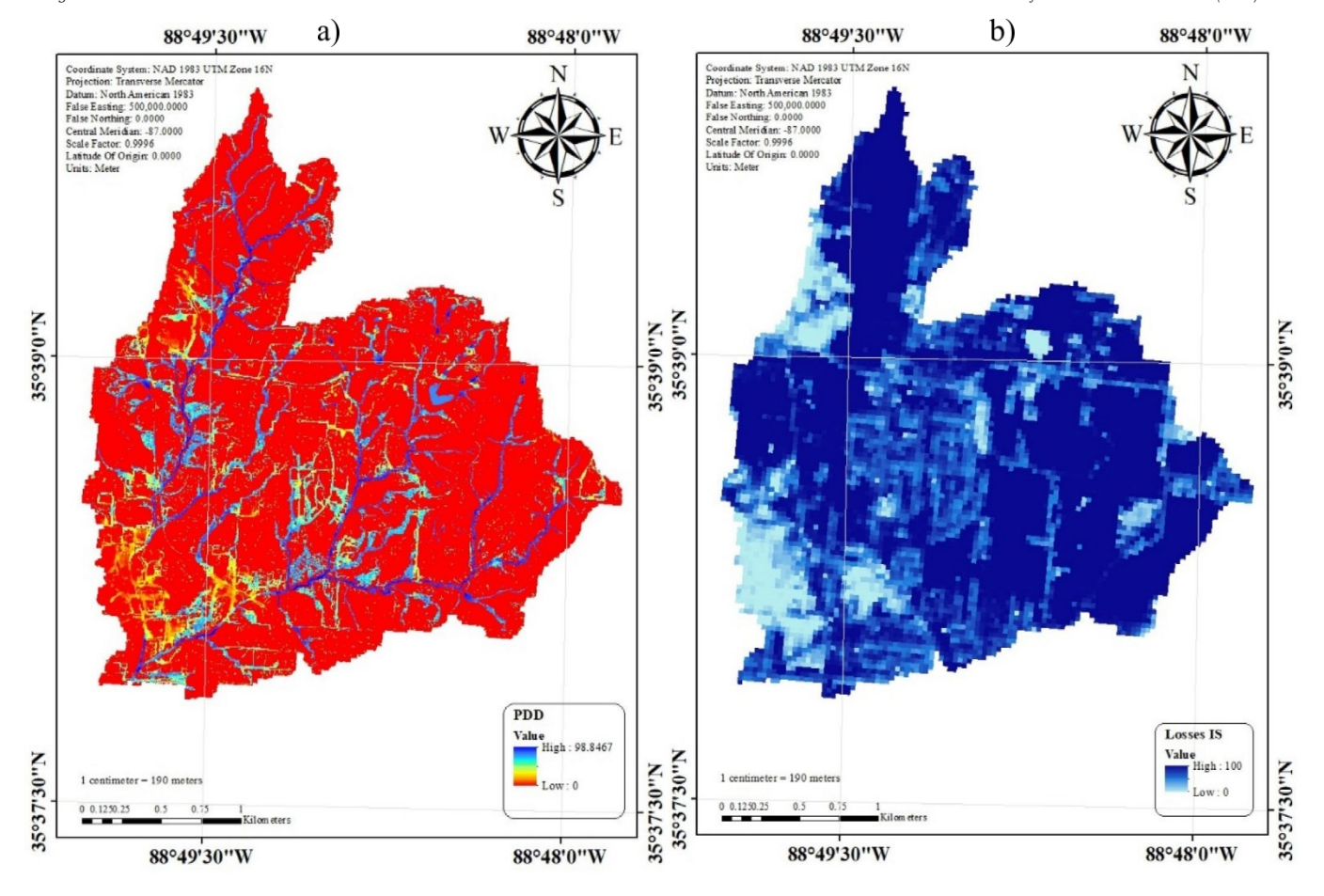


Fig. 13. a) The standardized map for flood depth distribution, b) The standardized map for the distribution of the impervious surface.

The spatial distribution of soil moisture across the study area versus the standard one is illustrated in Fig. 8. Since this study was first accomplished to assess the urbanization effects on the recharge process, we analyzed the land surface and river network's contribution to recharge into the aquifer using MODFLOW. Figs. 9 and 10 indicate the contribution of the land surface and river network to the total inflow in the Muse Street and Westwood zones, respectively.

Table 1 summarizes the results for the contribution of individual recharge components to the total inflow. According to this table (Table 1), urbanization decreased the natural recharge into the aquifer while the leakage from the riverbed remained constant. Also, urbanization decreased approximately 30 % of the total inflow into the groundwater. It is worth noting that Table 1 represents the total leakage from the riverbed and percolation from land surfaces across the studied basins.

The two-dimensional flood volume for a historic 24-h rainfall event of 242.2 mm with a 100-year return period was simulated using TUFLOW. The computational base hydrograph was also established by the SCS method, which devoted 20 min as the precipitation duration (Fig. 11). Finally, the hydraulic model was implemented in Aquaveo SMS once the precipitation volume was achieved.

The results of the hydraulic model, in the initial step, indicated good accordance with the maximum discharge and a relative difference with peak discharge volume as well as time to peak. These differences can be attributed to the weakness of flood routing in the hydraulic method and the different methods applied to calculate losses in SCS-CN. Also, differences might be referred to the hydraulic equations of two-dimensional TUFLOW, which was applied under two different conditions of losses,

including the Initial (IL) and Continuous Losses (CL). Table 2 shows the initial and continuous losses corresponding to the various land covers.

## 3.2. Soil water storage capacity in the base distribution

Fig. 12 shows the spatial map for the historic flow depth (moisture) distribution implemented under PMP across the study area. The graphs in gray and blue colors, respectively, represent outflow and in-flow corresponding to the PMP amount. The amount of saturated moisture was determined using linear regression. The maximum and minimum moisture was allocated to the location with maximum (equivalent to Sandy Creek West Wood sensor point) and minimum flow depth, respectively.

Fig. 13a and b illustrate the spatial distribution for flood depth as the initial output of the TUFLOW and infiltration, respectively, which were the basis for determining the soil water storage capacity distribution across the basin. All the components were standardized using fuzzification in GIS to develop a distinct index to assess the basin moisture conditions. This way, their initial domain was changed to a new one between 0 and 100, referring to the components' low and high values.

Fig. 14 illustrates the basin water storage capacity obtained by spatial composition of the standardized flood depth and impervious surfaces presented in Fig. 13a and b proceeds in GIS, respectively. According to this figure, the maximum and minimum values of 40 % and 1 % were respectively obtained from the southern parts of the aquifer close to the Sandy Creek West Wood sensor and the areas with low permeability or flood depth close to zero.

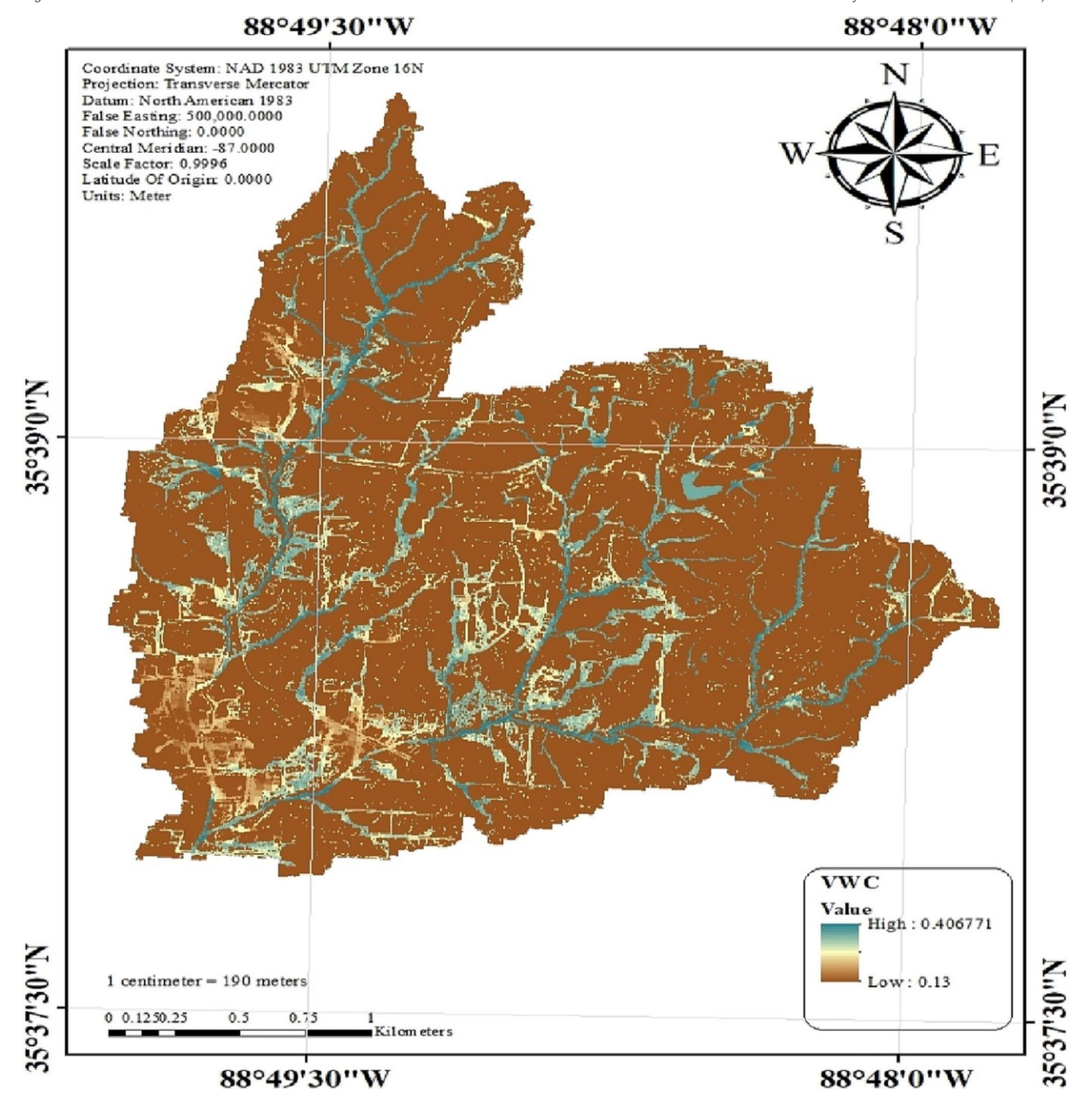


Fig. 14. The spatial map of soil water retention capacity coefficient (Sb) within the study area.

Fig. 15 depicts the results for the TUFLOW based on the effective flood magnitude of the SCS-CN equations (Appendix, Fig. 16). This figure illustrates the spatiotemporal variations of the probable maximum flood from its start to reach the peak.

Fig. 17 shows the soil storage index  $(\bar{\Phi}_{sc})$  versus soil moisture ratio (W/P) indices resulting from the standard and modified SCS-CN methods using the theoretical model and in-situ SWC sensors data. This figure shows a distinct difference between the estimated maximum soil moisture ratio and soil storage indexes resulting from the standard and modified SCS-CN methods. Such a difference implied that soil storage was satisfied soon through modified SCS-CN compared to the standard SCS-CN.

#### 3.3. First-order analysis of the basin shape reliability

Depending on the basin form factor, a natural classification with a median limit was used on the form factor (a) extent to investigate the effect of the distribution index. Therefore, the values of a = 0.2371, a = 0.4732, and a = 1.2361, as well as their equivalent distributions, were used to determine the mean and standard deviation of the  $\beta$  probability distribution. The closest fit to data was achieved at  $\beta$  = 1 and  $\alpha$  = 5. Fig. 18 depicts the division for basin form factor between 0 and 2.

Table 3 summarizes the statistics (mean and standard deviation) for the basin form factor obtained by the modified SCS-CN method, as presented in Fig. 18 (X2 values). Also, this table includes the correlation coefficient that

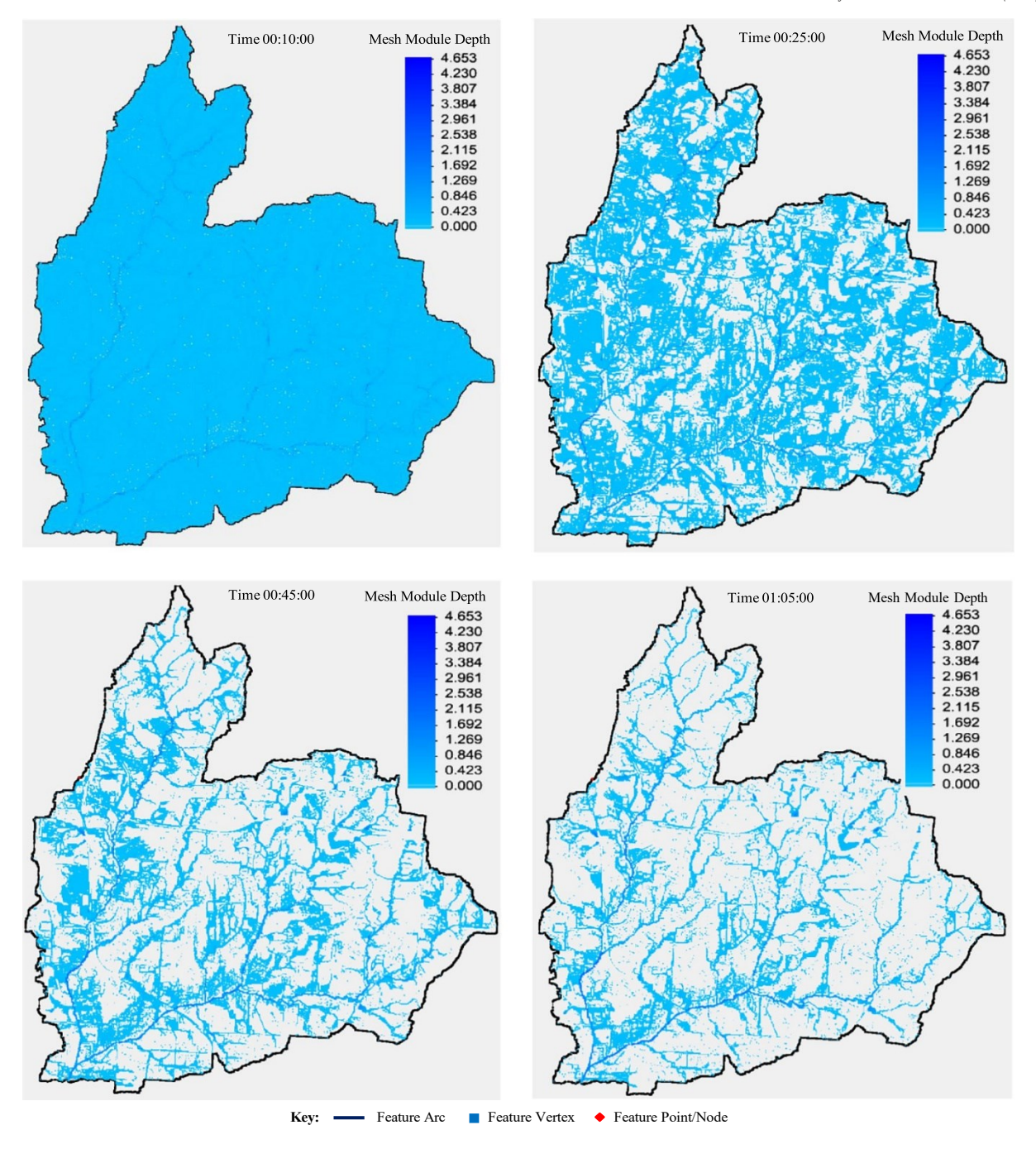


Fig. 15. Two-dimensional distribution of net flood from initiates to reach the peak.

corresponds to the experimental value resulting from standard SCS-CN calculations (X1 values). According to Table 3 of the performance assessment criteria results, the maximum correlation between modified and standard SCS-CN methods was shown when the form factor (a) was equal to 0.4732.

Fig. 19 shows the distribution of the finite state function of the randomly generated value for the two variables of X1 and X2 corresponding to the different amounts of the form parameters (a1, a2, and a3). These random values were generated using coding in Python 3.8. Afterward, the form factor was estimated using the calculated values as summarized and presented in Table 4.

According to the results of the first-degree linear function, X1-X2, it is expected that the failure threshold will happen with the probabilities of 55.235 %, 53.79 %, and 34.203 % corresponding to the basin form

factor values including a=0.2371, a=0.4732 and a=1.2361 (50 % base). Therefore, the equivalent discharge was calculated as presented in Table 5.

The SCS synthetic unit hydrographs resulting from the hydraulic model output, which were calibrated using standard and modified SCS-CN methods, are presented in Fig. 20. While the standard and modified SCS-CN methods are from the same family, they estimated different flood volumes due to the basin form factor (a) that the modified SCS-CN benefits. According to Fig. 19, the modified SCS-CN method accurately captured the soil moisture dynamics. Also, the simulation hydrograph using SCS-CN and TUFLOW hydraulic model followed the same pattern; however, there's a delay in their time to peak. Their differences in time to peak can be attributed to the different methods to estimate losses and the lack of flood rutting

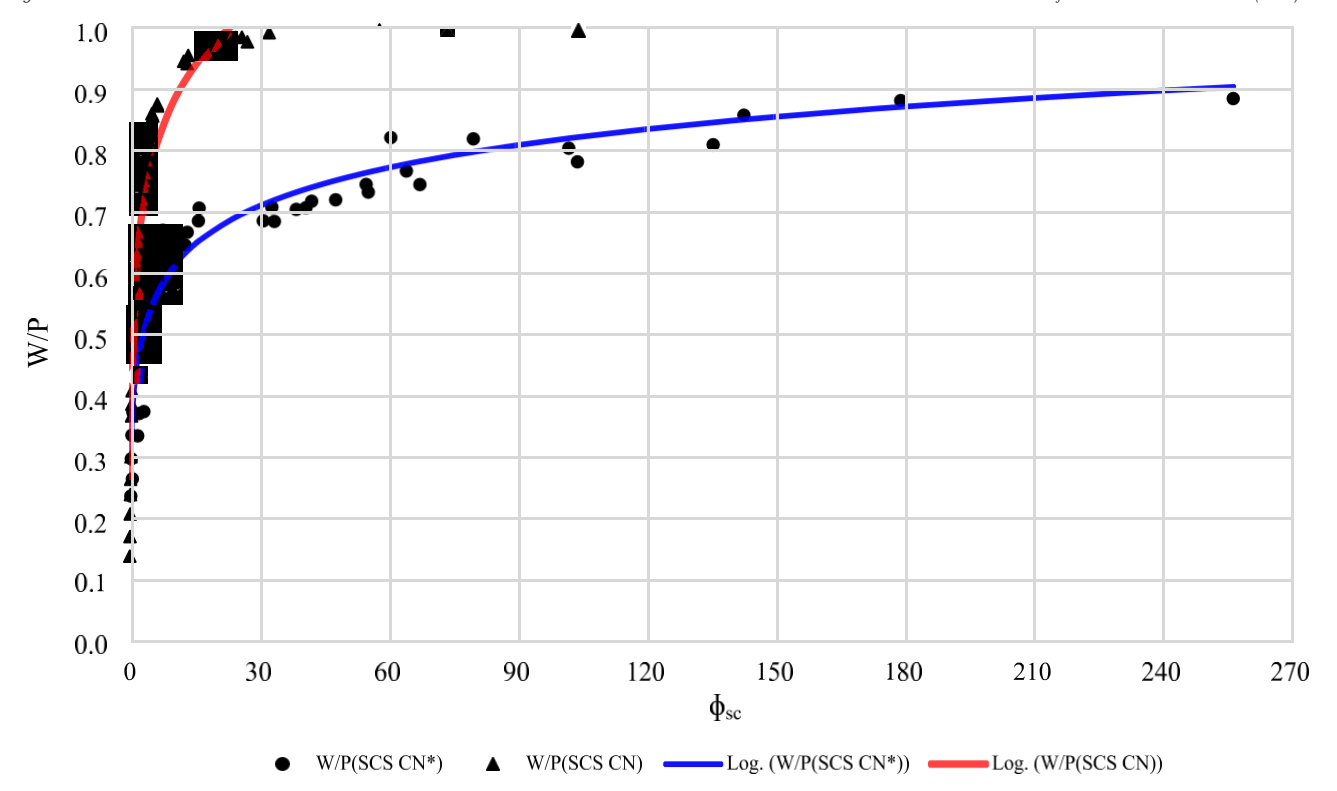


Fig. 17. Distribution of soil water storage capacity index ( $\bar{\varphi}_{sc}$ ) versus soil moisture ratio (W/P) obtained from the standard (Blue-colored) and modified (Red-colored) SCS-CN methods using the theoretical model and VWC sensor data.

process in the hydraulic method. Table 6 represents the statistical summary of the simulation processes using the standard and modified SCS-CN.

Table 6 represents different values for the flow volumes simulated by the hydraulic model using the standard and modified SCS-CN. The flow volumes based on the modified SCS-CN simulation were substantially higher than those obtained by applying the standard SCS-CN method as the continuous losses. It means that the modified SCS-CN intensified the flow volume

as the vital information in designing and establishing any construction downstream by supporting more safety. Table 6 illustrates valuable points regarding in- and out- peak flow as the initial losses. Accordingly, the 439.6  $\,\mathrm{m}^3/\mathrm{s}$  in-flow during the initial losses led to approximately  $15~\mathrm{m}^3/\mathrm{s}$  peak outflow under the standard SCS-CN method. While for the  $410.2~\mathrm{m}^3/\mathrm{s}$  as an inflow, a slightly high peak outflow was shown under the modified SCS-CN simulation.

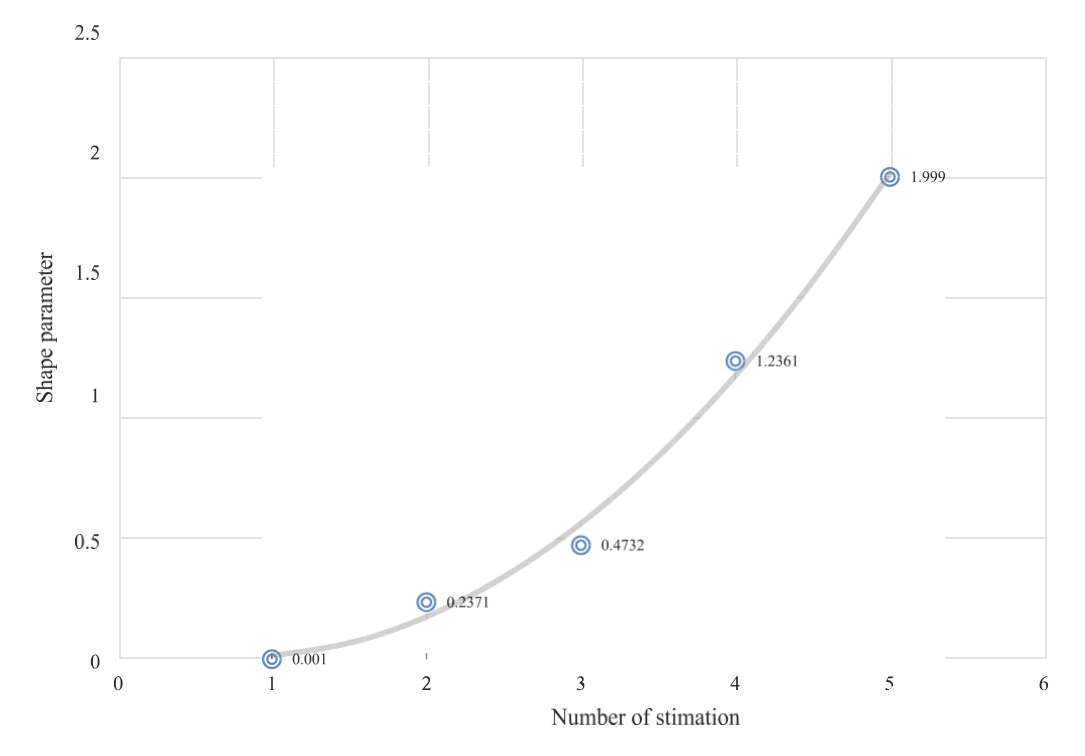
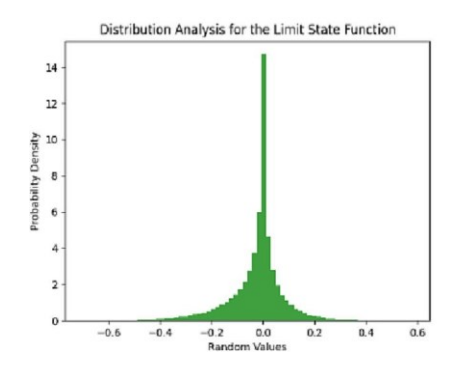
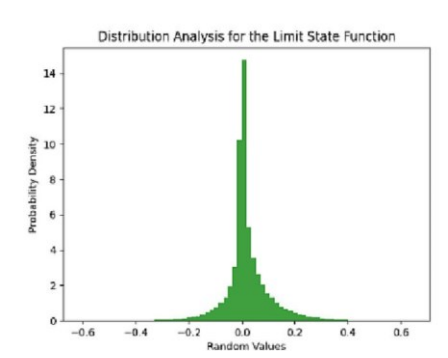


Fig. 18. The classification for the basin form factor based on possible limits and average initial value (Wang, 2018).

Table 3
The performance criteria results values presented by Wang (2018)

Shape Parameter	$\mathbb{R}^2$	STD (SCS CN*)	Mean (SCS CN*)	STD (SCS CN)	Mean (SCS CN)
a1 = 0.001	0.592627193	0.132750789	0.897195387	0.097593923	0.929182879
a2 = 0.2371	0.593103016	0.125241150	0.905617675		
a3 = 0.4732	0.593338096	0.116978677	0.914602541		
a4 = 1.2361	0.587654023	0.082957795	0.948820629		
a5 = 1.999	0.279731626	0.026494084	0.999091017		
	X2			X1	





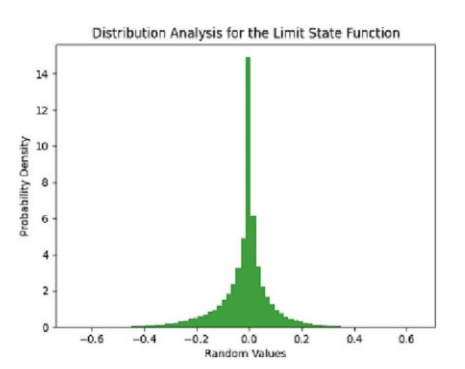


Fig. 19. Generated random data based on the mean and standard deviation for the first to third distribution from left to right.

The TUFLOW performance evaluation results showed 0.4916 as Nash–Sutcliffe in the standard SCS-CN method, while it was increased to 0.6890 in the modified SCS-CN. This difference can be attributed to the accuracy of calculated basin shape reliability at a = 0.473. Accord- ing to the results, the closest value to the basin form factor for all the separated individual events occurred at a = 0.417. Our results here are in accordance with Bartlett et al. (2016) which found that their mod- ified SCS-CN method shows higher performance in the simulation of the surface runoff than the standard SCS-CN method.

According to the results (Table 7), the same results for the soil water storage capacity were shown for both standard and modified SCS-CN methods. It means that, while these methods resulted in different flood volumes, the flood distribution across the region, which specifies soil water storage capacity, remained constant. The results suggest the river network enhancement resulting from increased impermeable surfaces would not lead to aquifer recharge.

# 4. Conclusion

This study was established to assess the effects of increased impervious surfaces and the likely excess overflow through the river network on recharge rates. We employed the TUFLOW hydraulic code to capture the runoff distribution change and evaluate the river network's recharge dynamics. To this end, we estimated the soil water storage capacity of the basin under two different conditions, with and without probability distribution functions, namely modified and standard SCS-CN.

The SCS synthetic unit hydrograph was also developed to calibrate the hydraulic model. The accuracy of the SCS synthetic unit hydrograph in overland flow estimation and its propagation completely depends on the

Table 4
Summary of the results of the FORM reliability analysis

Name	me DISTRIBUTION ANALYSIS		SIMULATION		
	Number of	Approximated	Reliability	Coefficient of	
	Simulations	Number of Bins	Index Beta	Variation of Pf	
a1 a2	10,000	72	-0.095236638 -0.131601303	0.026198104 0.028258824	

relationship between soil moisture capacity, effective rainfall conversion equations, and the surface runoff hydrograph equation parameters, respectively. In comparison, flood propagation is affected by the morphological conditions, mainly the soil water storage capacity of the catchment. A probabilistic method of reliability analysis (FORM) and the Importance Sampling (IS) approach were employed to estimate the threshold changes of the maximum possible discharge at the basin. Afterward, the estimated distribution equations were applied to calculate losses in the standard SCS-CN method, eventually leading to the initial accuracy of the basin shape parameter. This method (FORM) works based on the sensitivity recognition of the basin form factor through the basic distribution equations to estimate the percolation rate in the standard SCS-CN by the new cumulative distribution probability of soil moisture capacity in the catchment. Therefore, the calibrated simulations were used concerning the observed independent soil moisture and water storage capacity. Then, through the reliability analysis of the FORM factor using a linear performance function, the probability of a maximum flood event was estimated for the study region. In other words, the in-suit soil moisture records were expanded to the entire basin using a continuous standardized two-dimensional runoff (TUFLOW outputs) along with the impermeability values. Such generalization allowed us to estimate the flood volume using the reliability of FORM analysis based on distribution losses equations of the standard SCS-CN method. According to our findings, while considering a probability distribution function can estimate the soil water storage capacity of the region differs from the standard SCS-CN equations, flow distribution shape during historic floods across the basin remains a multiplier of low-intensity events.

Also, the findings suggest that the construction design based on modified SCS-CN will guarantee much more safety for human systems than the standard SCS-CN-based design since the soil water storage capacity was satisfied soon through modified SCS-CN approach leading to high peak discharge and flood volume for the same precipitation event. Hence, designing any construction, mainly dams downstream, using the modified SCS-CN

Table 5
Failure probability values correspond to the different amounts of basin form factor

a1	a2	аЗ
55.235 %	53.794 %	34.203 %

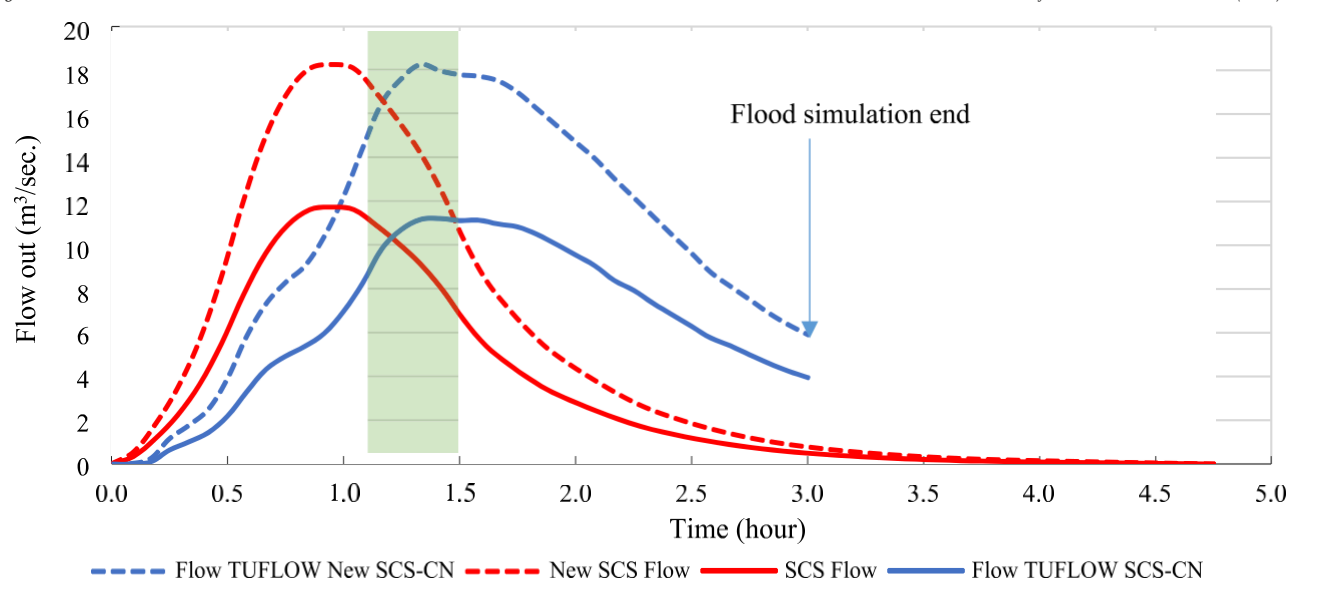


Fig. 20. PMF for the 6-h synthetic unit hydrograph in the extent of two possible thresholds.

Table 6 Statistical summary of the difference in outflow rate of the TUFLOW model

Aquaveo SMS TUFLOW Model Summary			Aquaveo SMS TUFLOW Model Summary				
SCS-CN				SCS-CN*			
Peak Flow In (m3/s)	439.6	IL	13.371	Peak Flow In (m3/s)	410.2	IL	0.656
Peak Flow Out (m3/s)	14.9			Peak Flow Out (m3/s)	16.7		
Volume at Start (m3)	0			Volume at Start (m3)	0		
Volume at end (m3)	69,226	CL	26.609	Volume at end (m3)	70,037	CL	29.571
Total Volume In (m3)	158,534			Total Volume In (m3)	166,205		
Total Volume Out (m3)	89,163			Total Volume Out (m3)	96,109		

method will provide more safety, particularly in crowded regions. The findings implied that the excess overflow resulting from the impervious surface into the river network leaves the region without increasing the recharge into the aquifer.

#### CRediT authorship contribution statement

A.N. Giglou: conceptualization, methodology development, data collection and processing, calculations and estimations, writing-original draft, and editing; R.R. Nazari: conceptualization, design, writing review, and editing; F. Jazaei: conceptualization, design, methodology development, writing review, and editing; M. Karimi: writing, review; and editing.

## Data availability

Data are available after a request from the corresponding author.

Table 7 Statistical summary of the difference in soil storage capacity estimated by standard and modified SCS-CN  $\,$ 

Soil Water Storage Capacity on SCS-CN Equ	Layer Based	Soil Water Storage Capacity Layer Based on SCS-CN* Equ		
Number of layered raster cells	1,136,244	Number of layered raster cells	1,136,244	
Minimum amount	0.130	Minimum amount	0.130	
Maximum amount	0.40	Maximum amount	0.40	

#### Declaration of competing interest

There is not any competing interest.

# Acknowledgments

This research was supported by the Center for Applied Earth Science and Engineering Research, the University of Memphis, during my post-doctoral fellowship, and I would thank Prof. Daniel Larsen, William Allen Simco, Spencer R Smith, and Jarod Przybylski for providing the streamflow and all necessary data which are available through the University of Memphis ETD system. This work was also supported through a grant from National Science Foundation (NSF) FII Track-2 FEC award No. 2217824.

#### Funding

Not applicable.

# Ethical approval

All authors declare that they have no conflict of interest.

## Consent to participate

Total amount	186.706	Total amount	187.031
Average value	0.164	Average value	0.164
Standard deviation	0.745	Standard deviation	0.750

Consent to publish

All authors approved the submission and consented to publication.

#### Appendix A

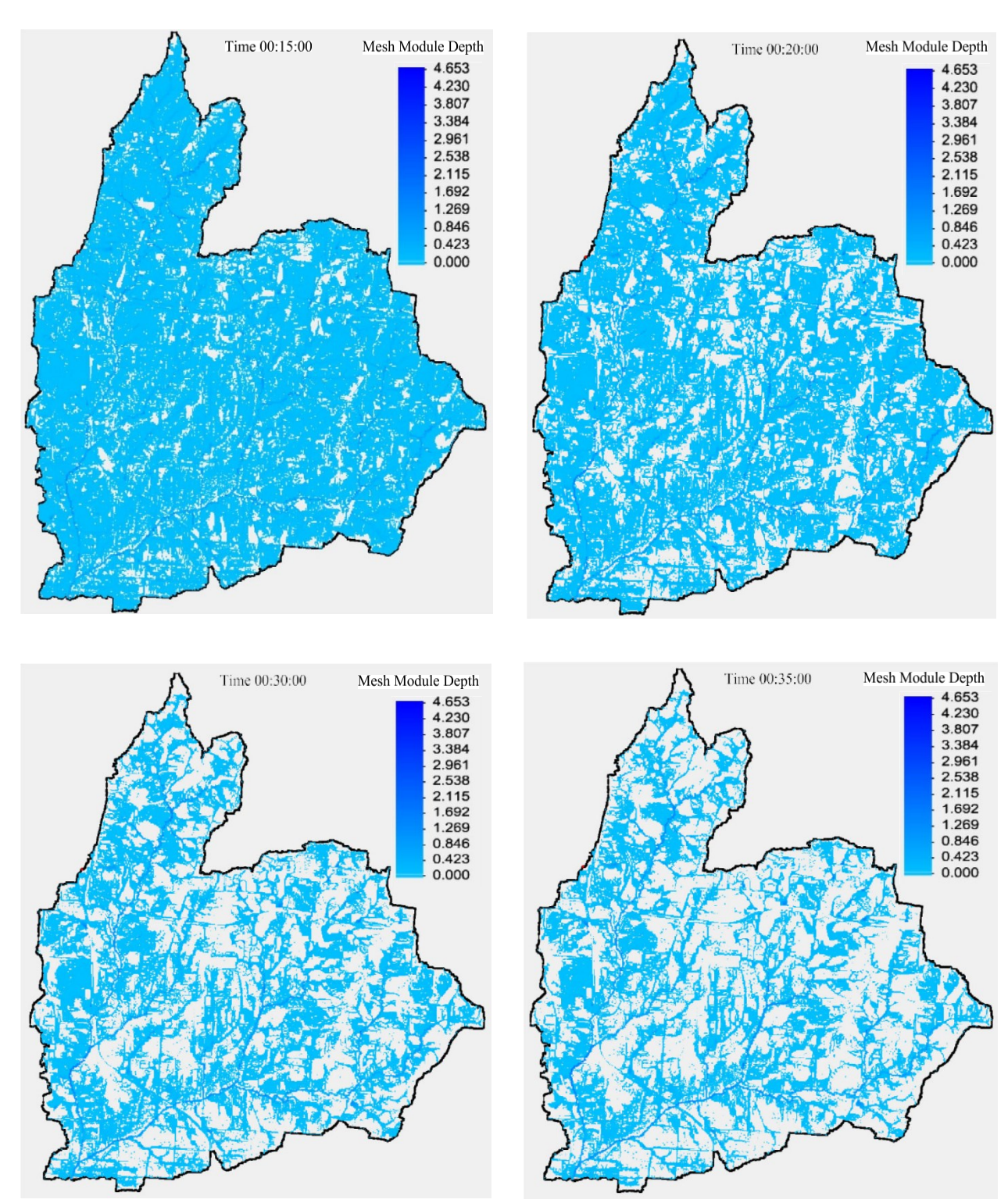


Fig. 16. Two-dimensional distribution of net flood from initiates to reach the peak.

# References

Ayalew Yifru, B., Chung, L.L.M., Kim, M.-G., Change, S.W., 2022. Assessing the Effect of Urbanization on Regional-scale Surface Water-groundwater Interaction and Nitrate Transport. 12, p. 12520. https://doi.org/10.1038/s41598-022-16134-1. Baker, Jack, 2010. CEE 204: Structural Reliability. Lecture Notes. Stanford University.

Bartlett, M.S., Parolari, A.J., McDonnell, J.J., Porporato, A., 2016. Beyond the SCS-CN method: a theoretical framework for spatially lumped rainfall-runoff response. Water Resour. Res. 52, 4608–4627.

Faber, M.H., 2009. Risk and Safety in Engineering. SS 2009. Lecture Notes. Swiss Federal Institut of Technology Zurich, Switzerland.

Fahad, M.G.R., Nazari, R., Motamedi, M.H., Karimi, M., 2020. Coupled hydrodynamic and geospatial model for assessing resiliency of coastal structures under extreme storm

- scenarios. Water Resour. Manag. 34, 1123–1138. https://doi.org/10.1007/s11269-020-02490-v.
- Fathi Nafchi, R., Yaghoobi, P., Vanani, H.R., Ostad-Ali-Askari, K., Nouri, J., Maghsoudlou, B., 2021. Eco-hydrologic stability zonation of dams and power plants using the combined models of SMCE and CEQUALW2. Appl. Water Sci. 11, 109.
- Feng, B., Zhang, Y., Bourke, R., 2021. Urbanization impacts on flood risks based on urban growth data and coupled flood models. Nat. Hazards 106, 613–627.
- Guan, M., Sillanpää, N., Koivusalo, H., 2016. Storm runoff response to rainfall pattern, magnitude and urbanization in a developing urban catchment. Hydrol. Process. 30, 543–557.
   Healy, R.W., Cook, P.G., 2002. Using groundwater levels to estimate recharge. Hydrogeol. J.
- 10, 91–109. https://doi.org/10.1007/s10040-001-0178-0. HEC, 2020. Technical Reference Manual. US Army Corps of Engineers. Institute for Water Re-
- sources. Hydrologic Engineering Center, 609 Second Street.

  Huntington, J.L., Niswonger, R.G., 2012. Role of surface-water and groundwater interactions on projected summertime streamflow in snow dominated regions: an integrated model-
- ing approach. Water Resour. Res. 48 (11). https://doi.org/10.1029/2012WR012319. Jazaei, F., Waldron, B., Schoefernacker, S., Larsen, D., 2019. Application of numerical tools to investigate a leaky aquitard beneath urban well fields. Water 11 (1), 5.
- Karimi, M., Nazari, R., Vant-Hull, B., Mittenzwei, M., Khanbilvardi, R., 2017. Predicting surface temperature variation in urban settings using real-time weather forecasts. J. Urban Clim. 20, 192–201. https://doi.org/10.1016/j.uclim.2017.04.008 Elsevier.
- Kloek, T., Dijk, H.K., 1987. Bayesian Estimates of Equation System Parameters: An Application of Integration by Monte Carlo. Econometrica 46 (1), 1–19.
- Kumar, R., Qureshi, M., Vishwakarma, D.K., Al-Naseri, N., Kuriqi, A., Elbeltagi, A., Saraswat, A., 2022. A review on emerging water contaminants and the application of sustainable removal technologies. Case Stud.Chem.Environ.Eng. 6, 100219.
- Lerner, D.N., Issar, A.S., Simmers, I., 1990. Groundwater recharge: a guide to understanding and estimating natural recharge. International Contributions to Hydrogeologists. 10. Imternational Association of Hydrogeologists, Goring, UK.
- Lian, H., Yen, H., Huang, Jr.Ch., Feng, Q., Qin, L., Bashir, M.A., Wu, Sh., Zhu, A.X., Luo, J., Di, H., Lei, Q., Liu, H., 2020. CN-China: revised runoff curve number by using rainfall-runoff events data in China. Water Res. 177, 115767.
- Lü, X., Han, Z., Li, H., Zheng, Y., Liu, J., 2022. Influence of urbanization on groundwater chemistry at Lanzhou Valley basin in China. Minerals 12, 385. https://doi.org/10. 3390/min12030385.
- Markstrom, S.L., Niswonger, R.G., Regan, R.S., Prudic, D.E., Barlow, P.M., 2008. GSFLOW—Coupled groundwater and surface-water flow model based on the integration of the Precipitation-Runoff Modeling System (PRMS) and the Modular Ground-Water Flow Model (MODFLOW-2005): U.S. Geological Survey Techniques and Methods 6-D1. p. 240.
- McGrane, S.J., 2016. Impacts of urbanisation on hydrological and water quality dynamics, and urban water management: a review. Hydrol. Sci. J. 61, 2295–2311.
- Melchers, R.E., 1999. Structural Reliability—Analysis and Prediction. Ellis Horwood Limited, Chichester, UK.
- Mockus, V., 1972. National Engineering Handbook Section 4, Hydrology. NTIS.
- Nazari, R., De Hoyos, S., Khanbilvardi, R., 2013. Freshwater demands and shortages. Encyclopedia of Crisis Management. SAGE Publications ISBN: 9781452275956.

- Ostad-Ali-Askar, K., 2022. Review of the effects of the anthropogenic on the wetland environment. Appl. Water Sci. 12, 260.
- Pasquier, U., Vahmani, P., Jones, A.D., 2022. Quantifying the city-scale impacts of impervious surfaces on groundwater recharge potential: an urban application of WRF–Hydro. Water 14, 3143. https://doi.org/10.3390/w14193143.
- Perez, A.J., Abraho, R., Causpe, J., Cirpka, O.A., Burger, C.M., 2011. Simulating the transition of a semi-arid rainfed catchment towards irrigation agriculture. J. Hydrol. 409, 663–681.
- Ponce, V., 1996. Notes of My Conversation With Vic Mockus unpublished material, (last access: 29 September 2017).
- Rosburg, T.T., Nelson, P.A., Bledsoe, B.P., 2017. Effects of urbanization on flow duration and stream flashiness: a case study of Puget Sound Streams, Western Washington, USA. J. Am. Water Resour. Assoc. 53, 493–507.
- Ryan, Ph., Syme, B., Gao, Sh., Collecutt, G., 2022. Direct rainfall hydraulic model validation. Hydrology and Water Resources Symposium. ISBN: 978-1-925627-64-0.
- Scanlon, B.R., Healy, R.W., Cook, P.G., 2002. Choosing appropriate techniques for quantifying groundwater recharge. Hydrogeol. J. 10, 18–39. https://doi.org/10.1007/s10040-001-0176-2
- Schoener, G., Stoneb, M.C., 2019. Impact of antecedent soil moisture on runoff from a semiarid catchment. J. Hydrol. 569, 627–636. https://doi.org/10.1016/j.jhydrol.2018.12.025.
- Shi, W., Wang, N., 2020. An improved SCS-CN method incorporating slope, soil moisture, and storm duration factors for runoff prediction. Water 12 (5), 1335. https://doi.org/10.3390/w12051335.
- Shirmohammadi, B., Malekian, A., Salajegheh, A., Taheri, B., Azarnivand, A., Malek, Z., Verburg, P., 2020. Impacts of future climate and land use change on water yield in a semi-arid basin in Iran. Land Degrad. Dev. 31 (10), 1252–1264.
- Talebmorad, H., Ostad-Ali-Askari, K., 2022. Hydro geo-sphere integrated hydrologic model in modeling of wide basins. Sustain.Water Resour.Manag. 8, 118. https://doi.org/10.1007/ s40899-022-00689-y.
- Tian, H., Chen, G., Lu, Ch., Xu, X., Ren, W., Zhange, B., Banger, K., Tao, B., Pan, Sh., Liu, M., Zhange, Ch., Bruhwiler, L., Wofsy, S., 2015. Global methane and nitrous oxide emissions from terrestrial ecosystems due to multiple environmental changes. Ecosyst. Health Sustain. 1 (1), 4. https://doi.org/10.1890/EHS14-0015.1.
- Wang, D., 2018. A new probability density function for spatial distribution of soil water storage capacity leads to the SCS curve number method. Hydrol. Earth Syst. Sci. 22, 6567–6578.
- Wang, P., Lu, Z., Tang, Z., 2013. A derivative based sensitivity measure of failure probability in the presence of epistemic and aleatory uncertainties. Comput. Math. Appl. 65, 89–101.
- WBM, B., 2008. TUFLOW User Manual. GIS Based. BMT WBM, Australia.
- WBM, B., 2016. TUFLOW User Manual. GIS Based. BMT WBM, Australia.
- Wood, E.F., Lettenmaier, D.P., Zartarian, V.G., 1992. A land surface hydrology parameterization with subgrid variability for general circulation models. J. Geophys. Res. 97, 2717–2728.